# ASSIMILATION OF REAL-TIME DEEP SEA BUOY DATA FOR TSUNAMI FORECASTING ALONG THAILAND'S ANDAMAN COASTLINE

**Seree Supharatid**

Natural Disaster Research Center, Rangsit University, Pathumtani 12000, Thailand

## ABSTRACT

The occurrence of 2004 Indian Ocean tsunami enhanced the necessity for a tsunami early warning system for countries bordering the Indian Ocean, including Thailand. This paper describes the assimilation of real-time deep sea buoy data for tsunami forecasting along Thailand's Andaman coastline. Firstly, the numerical simulation (by the linear and non-linear shallow water equations) was carried out for hypothetical cases of tsunamigenic earthquakes with epicenters located in the Andaman micro plate. Outputs of the numerical model are tsunami arrival times and the maximum wave height that can be expected at 58 selected communities along Thailand Andaman coastline and two locations of DART buoys in the Indian Ocean. Secondly, a "neural" network model (GRNN) was developed to access the data from the numerical computations for subsequent construction of a tsunami database that can be displayed on a web-based system. This database can be updated with the integration from two DART buoys and from several GRNN models.

**Key words:** Numerical modeling, Neural network modeling, Web-based online, Data assimilation, GRNN, DART Buoy

*Science of Tsunami Hazards, Vol. 27, No. 3, page 30 (2008)*

## 1. Introduction

The 2004 Indian Ocean tsunami was responsible for the greatest damage in history and a death toll of more than 200,000 people. The highest number of victims (both confirmed dead and missing) was in Indonesia (163,795), followed by Sri Lanka (35,399), India (16,389) and Thailand (8,345)(International Federation of Red Cross and Red Crescent, 2005). In Thailand, many resorts in the low-laying coastal area of Kao Lak experienced serious destruction and more than 2,000 people lost their lives.

Because of the great damage and destruction caused by this 2004 disaster, it is necessary to review the present tsunami warning systems and examine three important aspects - specifically timing, accuracy and stability. Whitmore and Sokolowski (1996) developed the following approach in forecasting tsunami heights. They used a nonlinear long-wave numerical model to develop a database of water levels for 15 hypothetical tsunamigenic earthquakes in the northwest Pacific, for events ranging in moment magnitude from 7.5 to 9.0. According to this method, when a possible tsunamigenic earthquake occurs, a comparison of pre-computed and of measured water levels near the tsunamigenic source from the database helps identify the closest event and provides an estimate of tsunami heights for the Pacific. According to another numerical simulation technique introduced by the Japan Meteorological Agency (JMA) in April 1999(JMA, 2006), tsunami generation and propagation for 100,000 different cases (epicenter, depth, magnitude and fault geometry) are calculated in advance and the estimated tsunami heights and arrival times along the coast are stored in a database for use in the warning system. Still, another method for quick tsunami forecasting database for Korea (Lee et al., 2005), uses a superposition of a linear long wave solution which describes tsunami propagation from tsunami source units of 5.5 km. x 5.5 km. area and 1.0 height along the active fault zone in the Sea Japan/East Sea. Finally, NOAA's World Data Center A – Tsunami (WDC, 2005) has collected an updated tsunami database for the Atlantic, Indian, and Pacific Oceans, as well as the Mediterranean and the Caribbean Seas. This NGDC tsunami database - dating from 2000 B.C. to the present - includes a listing of historical tsunami source events and run-up locations throughout the world.

The first model simulation results of the Indian Ocean tsunami were obtained from the "MOST" (Method of Splitting Tsunamis) model (Titov and Synolakis, 1998) and were posted by Titov on the Internet Tsunami Bulletin Board (within 12 hours after the earthquake). MOST is part of the tsunami forecasting and warning system under development for the Pacific Ocean (Titov et al., 2005) that will provide fast real time estimates of tsunami amplitudes using preset models, real-time seismic data and, most importantly, deep-ocean tsunami amplitude data from a network of deep-ocean pressure sensors. Other researchers also ran models and posted results. Results of MOST and of other model runs have been widely used worldwide by the media for early planning of relief efforts and for post-tsunami field surveys. Unlike the Pacific, the Indian Ocean does not yet have a network of deep ocean pressure sensors, and so coastal tide gauges provide the only direct measurements of Indian Ocean tsunami amplitudes.

On May 30, 2005, five months after the December 26, 2004 tsunami, Thailand begun operating a National Disaster Warning Centre (NDWC, 2006) to monitor and relay critical information on all natural disasters. For the tsunami warning system, the NDWC begun using data on earthquake magnitude and depth for estimates of the potential risk from possible tsunamis. In November 2006, the NDWC, in cooperation with USAID, deployed the first DART buoy in the Indian Ocean. However, to establish an operating tsunami warning system, Thailand also required the development of a tsunami database along its Andaman Sea coastline.

The present study describes the development of a hybrid model that was developed by the integration of three techniques. First, a numerical model of linear and non-linear shallow water waves is introduced. Secondly, the neural network model is described in detail and the results of the database are displayed at an internet website. Thirdly, the database is updated with the assimilation from two DART buoys in the Indian Ocean, making use of several GRNN models.

## 2 Methodology

### 2.1 Numerical computation

A numerical model (similar to that of Shuto, 1997) was set up using linear and non-linear shallow water equations for estimation of tsunami propagation and of terminal effects. Equations. (1) – (3) are the linear equations without bottom friction in two-dimensional flow.

$$\frac{\partial \eta}{\partial t} + \frac{1}{R\cos\theta}\left(\frac{\partial M}{\partial \lambda} + \frac{\partial (N\cos\theta)}{\partial \theta}\right) = 0 \qquad (1)$$

$$\frac{\partial M}{\partial t} + \frac{gh}{R\cos\theta}\frac{\partial \eta}{\partial \lambda} = fN \qquad (2)$$

$$\frac{\partial N}{\partial t} + \frac{gh}{R}\frac{\partial \eta}{\partial \theta} = -fM \qquad (3)$$

Where $\eta$ is the vertical displacement of the water surface above still water level, R is the earth's radius, t is time , g is the gravitational acceleration, M and N are discharge fluxes in the $\lambda$ (along a parallel of latitude) and $\theta$ (along a circle of longitude) directions and f ($2\omega\sin\theta$) is the Coriolis coefficient.

Generally, a relatively smaller grid mesh is required to compute the tsunami along the coast where the water depth is shallow and variation of local topography has an important effect on tsunami behavior. However, it is difficult to use a smaller grid mesh in the total region of the large computational domain, such as the near shore of Thailand's Andaman coastline. Hence, the shallow water equations are applicable. The nonlinear shallow water equations in a Cartesian co-ordinate system consist of the continuity (Eq. (4)), and momentum equations in x (Eq. (5) and y (Eq. (6)):

$$\frac{\partial \eta}{\partial t} + \frac{\partial M}{\partial x} + \frac{\partial N}{\partial y} = 0 \qquad (4)$$

$$\frac{\partial M}{\partial t} + \frac{\partial}{\partial x}\left(\frac{M^2}{D}\right) + \frac{\partial}{\partial y}\left(\frac{MN}{D}\right) + gD\frac{\partial \eta}{\partial x} + g\frac{n^2}{D^{7/3}}M\sqrt{M^2+N^2} = 0 \qquad (5)$$

$$\frac{\partial N}{\partial t} + \frac{\partial}{\partial x}\left(\frac{MN}{D}\right) + \frac{\partial}{\partial y}\left(\frac{N^2}{D}\right) + gD\frac{\partial \eta}{\partial y} + g\frac{n^2}{D^{7/3}}N\sqrt{M^2+N^2} = 0 \qquad (6)$$

where “x” and “y” are horizontal coordinates, D is the total water depth, and n is Manning’s roughness. The application of the long-wave equations for tsunami modeling have also been described by Shuto et al. (1986), Kowalik and Murty (1993), and Titov and Synolakis (1998).

The computing domain covering the Andaman Sea coastline is shown in Fig. 1. The total region is bounded by latitude $2^{O}$ S longitude $85^{O}$ E to latitude $18^{O}$ N longitude $105^{O}$ E. Dynamic linking is accomplished in the boxed area. According to this method, larger grids in the deep sea are overlapped and dynamically linked with grids having 1/4 of the width in the shallower region (linking of 1.85 km to 462.5 m). During the computation, water level and discharge are exchanged satisfying a dynamic equilibrium along the boundary of these two regions. This process is repeated until the required grid resolution is obtained.

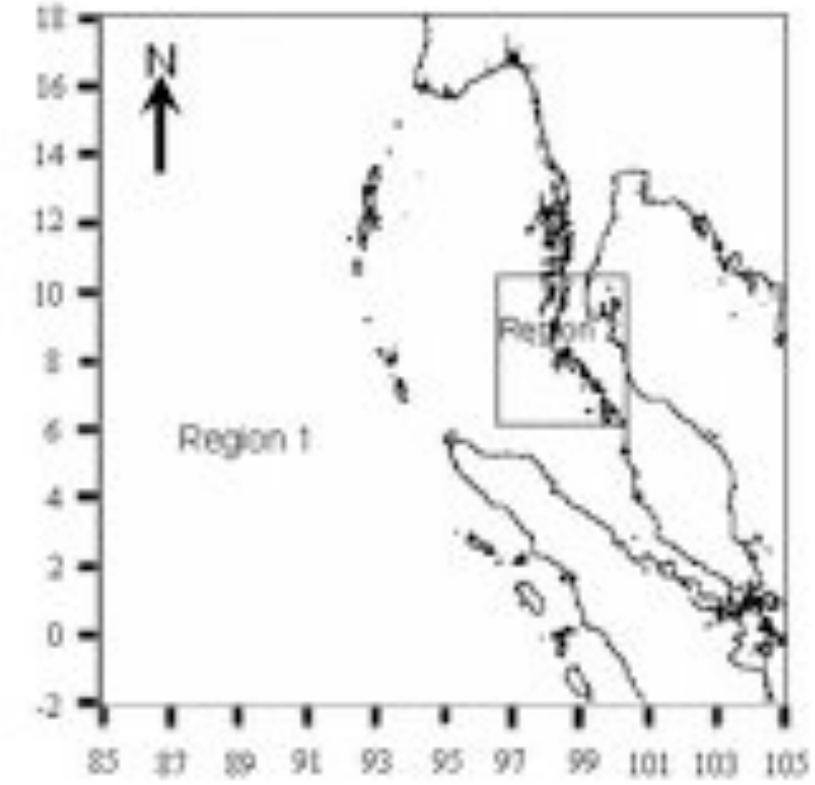


Fig. 1 Computing Domain

The initial condition corresponds to still water with the specified surface wave at the source of the earthquake. The algorithm of Mansinha and Smylie (1971) provides the initial surface wave through the seafloor deformation - based on input seismic parameters that include strike, dip and slip angles, the amount of the slip displacement and the location of the fault. The tsunami sources and earthquake epicenters for the Andaman micro plate were obtained from historic earthquakes (USGS) (Lay et al., 2005). Figure 2 shows the model region, which covers most of Thailand’s Andaman coastline with postulated earthquakes and tsunamis. Prior to the simulation, the model was calibrated with measurements of the tsunamis of 1881, 1941 and 2004.

The moment magnitude of postulated earthquakes was varied from 6.0 – 9.0. The relationship between moment magnitude and the fault dimensions were obtained from Donald and Kevin (1994) and Kanamori, H(1977). In total, there are 420 cases in the simulation.

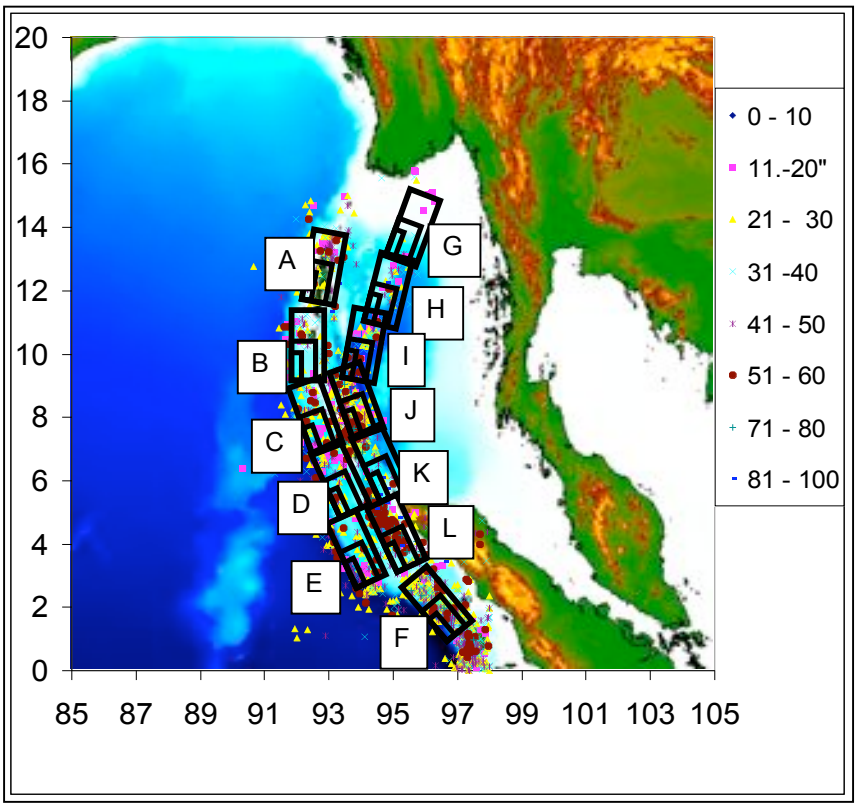


Fig. 2 Hypothetical earthquakes

**2.2 Neural network**

The neural network (NN) techniques used to solve problems in civil engineering began in the late 1980s (Flood and Kartam, 1994). Their applications in simulating and forecasting problems in oceanography are relatively recent (Hsieh and Pratt, 2001; Supharatid, 2003; Cigizoglu, 2005). Unlike other conventional-based models, the NN model is able to solve problems without any prior assumptions. As long as enough data is available, a neural network will extract any regularities or patterns that may exist and use it to form a relationship between input and output. Additional benefits include data error tolerance and the characteristic of being data-driven, thereby providing a capacity to learn and generalize patterns in noisy and ambiguous input data.

The General Regression Neuron Network (GRNN) proposed by Specht (1991) does not require an iterative training procedure as required in the back propagation method. It approximates any arbitrary function between input and output vectors, drawing the function estimate directly from the training data. In addition, it is consistent in that, as the training set size becomes large, the estimation error approaches zero with only mild restrictions on the function. The GRNN is used for the estimation of continuous variables, as in standard regression techniques. It is related to the

radial basis function network and is based on a standard statistical technique called kernel regression. The GRNN is a feed forward neural network best suited to function approximation tasks such as system modeling and prediction. It is a four-layer network with one hidden layer described in Fig. 3.

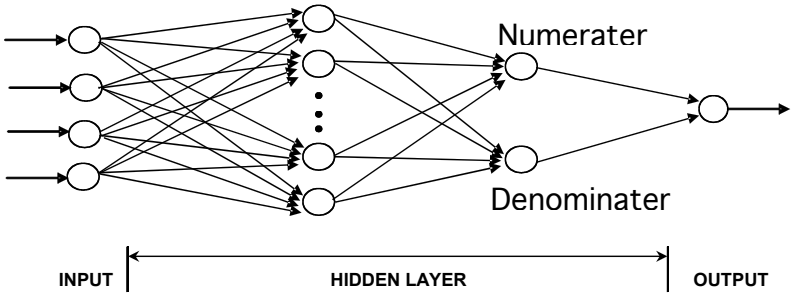


Fig. 3 Basic Procedure of GRNN

The input is a state space denoted by X (Epicenter, moment magnitude and earthquake depth). The estimated value ($\hat{Y}$) is calculated by Eq. (7) at 58 selected communities and 2 DART buoy locations (see Fig. 4). In this study, we used the cross training technique. Therefore, there are 210 hypothetical cases for training and 210 cases for testing the network. The input parameters are varied according to Table 1.

$$\hat{Y}(x) = \frac{\sum_{i=1}^{k} Y^i \exp(-D_i^2 / 2\sigma^2)}{\sum_{i=1}^{k} \exp(-D_i^2 / 2\sigma^2)} \qquad (7)$$

Where k is the number of input patterns is a scalar function representing the Euclidian square from the new input pattern to the training input pattern, and σ is a single smoothing parameter, which determines how tightly the network matches its prediction to the data in the training patterns.

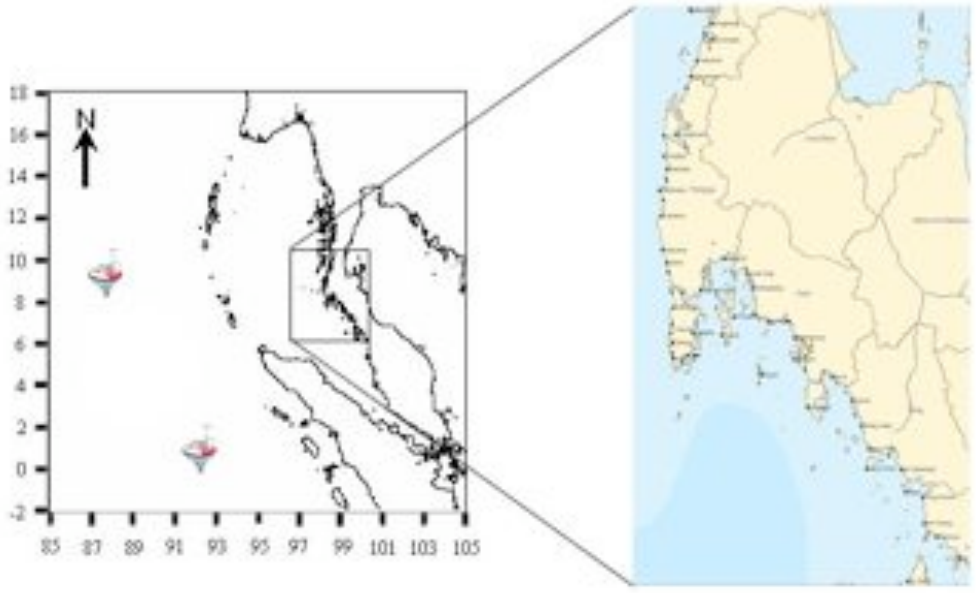


Fig. 4 Location of 58 selected communities and 2 DART buoys

Table 1 Input parameters and outputs for GRNN-1 model

| Inputs | | Outputs |
|---|---|---|
| Epicenter | Fixed at 12 locations | Maximum wave height in 58 risked communities along the coastline and 2 DART buoy locations |
| Earthquake magnitude (Mw) | 6.0, 6.5, 7.0, 7.5, 8.0, 8.5 and 9.0 | |
| Earthquake depth (D) | 10, 20, 30, 40 and 50 km. | |

By definition, the regression of a dependent variable y on an independent x, estimates the most probable value for y, given x and a training set. The regression method will produce the estimated value of y which minimizes the Mean-Squared Error (MSE). The GRNN is a method for estimating the joint probability density function (pdf) of x and y, given only a training set. Because the pdf is derived from the data with no preconceptions about its form, the system is perfectly general.

To evaluate the performance of GRNN, two common statistics, Efficiency Index (EI) and Root Mean Square Error (RMSE) are used as given in Eqs. (8) and (9).

$$EI = 1 - \frac{\sum_{k=1}^{k} (O_k - H_k)^2}{\sum_{k=1}^{k} (O_k - \overline{O})^2} \tag{8}$$

$$RMSE = \sqrt{\frac{\sum_{k=1}^{k} (O_k - H_k)^2}{k}} \tag{9}$$

where $O_p$ and $H_p$ are the target output and forecasted output, respectively. $\overline{O}$ is the mean value of the target output.

**2.3 Data assimilation**

In real operation, the initial warning decisions described in section 2.2 are based only on earthquake parameters. Without data assimilation from the direct measurement, results are susceptible to large errors of seismic source estimates. It has to be mentioned that the tsunami confirmation by coastal tide gages may come too late for timely evacuation measures. This can lead to a high false alarm rate and ineffective local emergency response. In this study, the arrival time of tsunami wave is detected by 2 DART buoys (see also Figure 4). The 1st and 2nd DART buoys were installed in the Indian Ocean at lat. $8.9^{O}$ N, long. $88.5^{O}$ E (No. 23401) and lat. $0.05^{O}$ N, long $81.88^{O}$ E (No. 54301), respectively. The previous GRNN-1 model was improved (GRNN-1.1, GRNN-1.2, GRNN-2). Difference in these models is the number and the position of DART buoys to be input to the model. Details of input are given in Tables 2 -4.

Table 2 Input parameters and outputs for GRNN–1.1 model

| Inputs | | Outputs |
|---|---|---|
| Epicenter | Fixed at 12 locations | Maximum wave height in 58 selected communities along the coastline |
| Earthquake magnitude (Mw) | 6.0, 6.5, 7.0, 7.5, 8.0, 8.5 and 9.0 | |
| Earthquake depth (D) | 10, 20, 30, 40 and 50 km. | |
| DART buoy | No. 23401 | |

Table 3 Input parameters and outputs for GRNN–1.2 model

| Inputs | | Outputs |
|---|---|---|
| Epicenter | Fixed at 12 locations | Maximum wave height in 58 selected communities along the coastline |
| Earthquake magnitude (Mw) | 6.0, 6.5, 7.0, 7.5, 8.0, 8.5 and 9.0 | |
| Earthquake depth (D) | 10, 20, 30, 40 and 50 km. | |
| DART buoy | No. 54301 | |

Table 4 Input parameters and outputs for GRNN–2 model

| Inputs | | Outputs |
|---|---|---|
| Epicenter | Fixed at 12 locations | Maximum wave height in 58 selected communities along the coastline |
| Earthquake magnitude (Mw) | 6.0, 6.5, 7.0, 7.5, 8.0, 8.5 and 9.0 | |
| Earthquake depth (D) | 10, 20, 30, 40 and 50 km. | |
| DART buoy | Nos. 23401 and 54301 | |

## 2. Discussion of Results

Some examples of the maximum simulated tsunami wave height for Case study A, D, F and J are depicted in Fig. 5. They are shown only for the earthquake of magnitude Mw 9 and depth of 10 km. It was found that in all cases the main energy lobe is directed perpendicular to the elongated source in the deep water. These figures also display the wave height enhancement in the shallow water and especially in proximity to 6 provinces along Thailand's Andaman coastline. Regions in the northwest of Thailand show considerable energy concentration through refraction process.

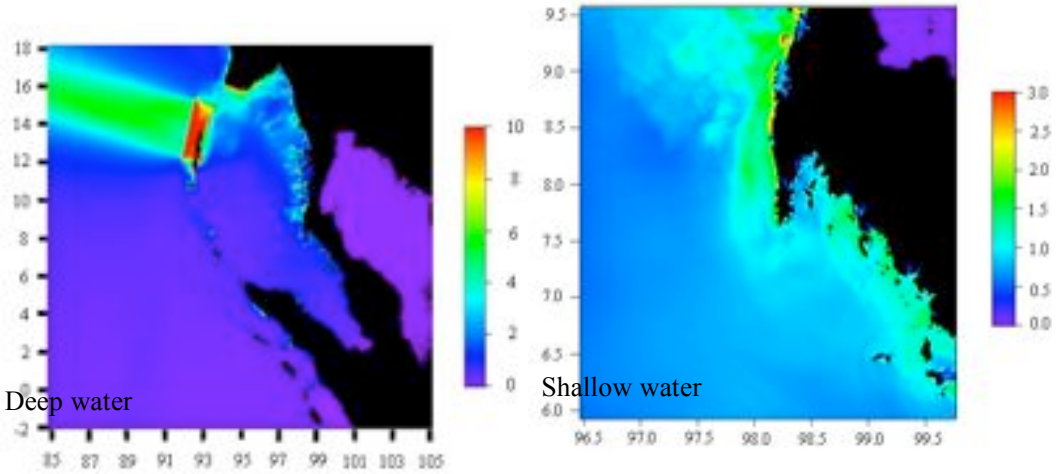


(a) Case A

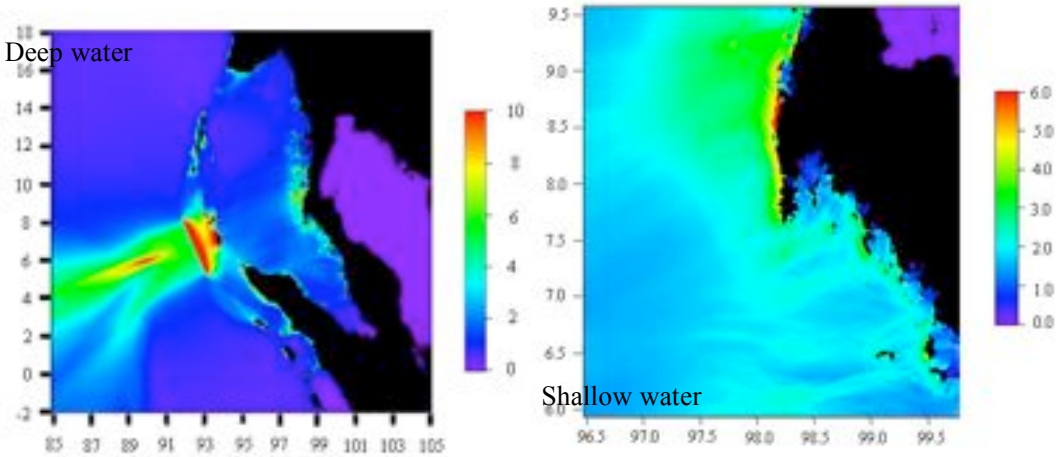


(b) Case D

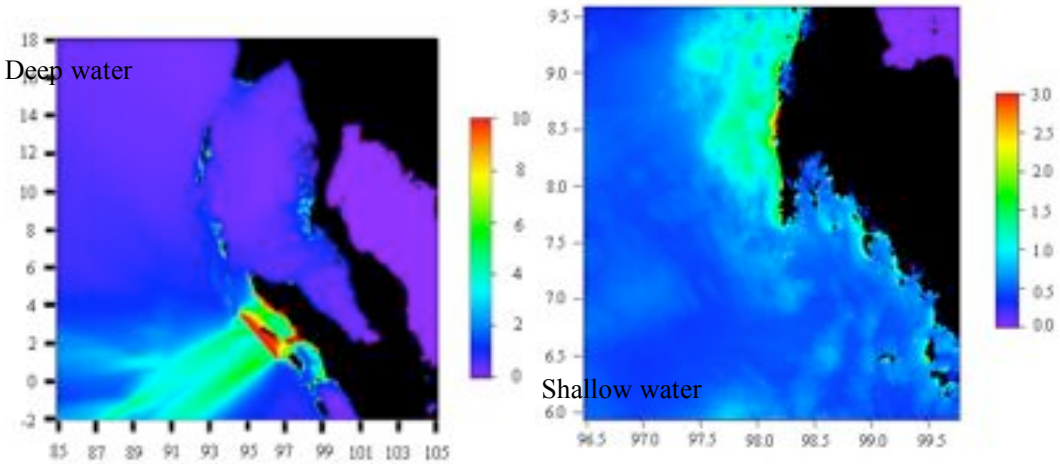


© Case F

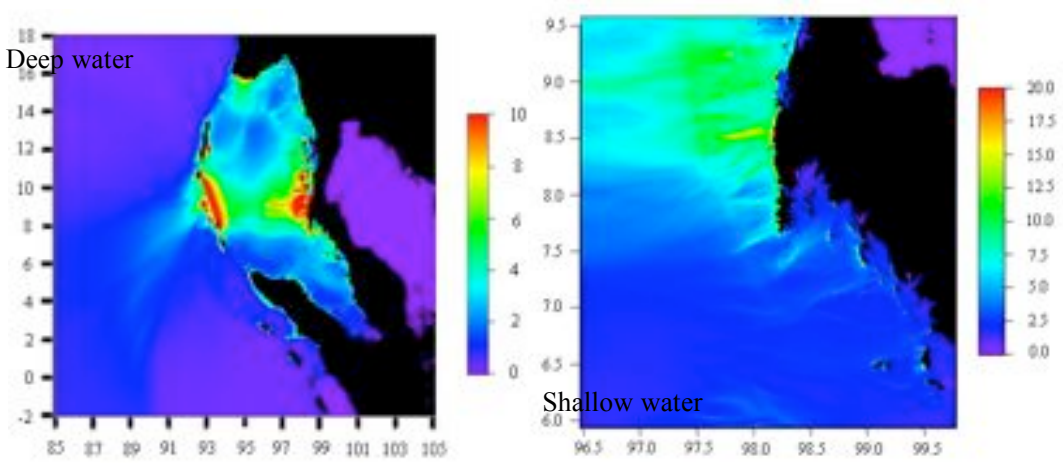


(d) Case J

Fig. 5 Maximum tsunami wave height

Figure 6 shows scatter plots of wave height at some communities (Talaenok, Namkem, Patong and Phiphi) and at 2 DART buoys in the Indian Ocean from the GRNN-1 model. Straight lines show perfect agreement. In general, agreements between the GRNN and numerical model are satisfactory with the EI more than 0.90 and RMSE less than 1 m. However, some deviations are found in medium to large wave heights (Most GRNN model gave underestimated results).

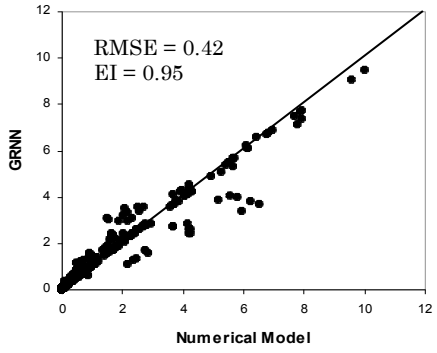


(a) Talaenok

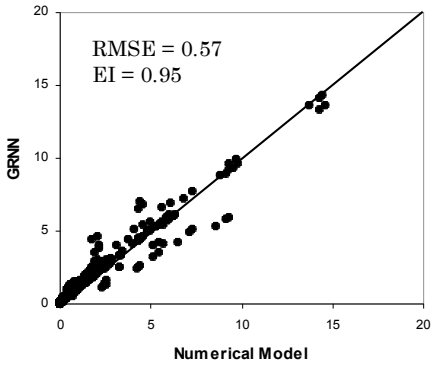


(b) Namkem

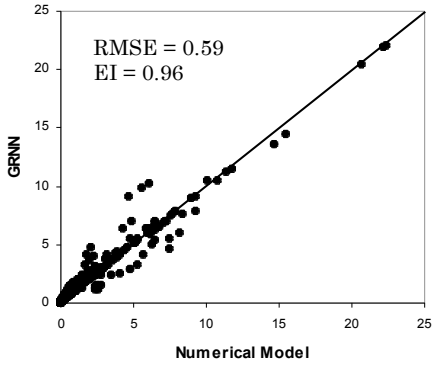


(c) Patong beach

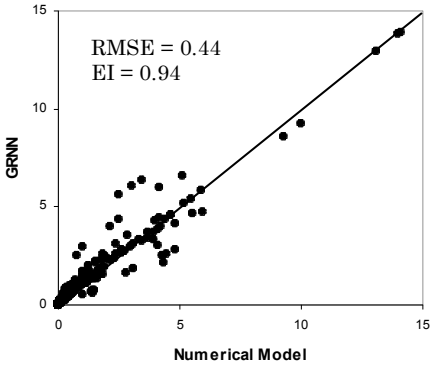


(d) Phiphi Island

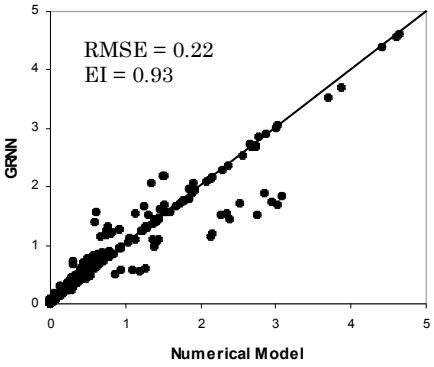


(e) Ao Makam

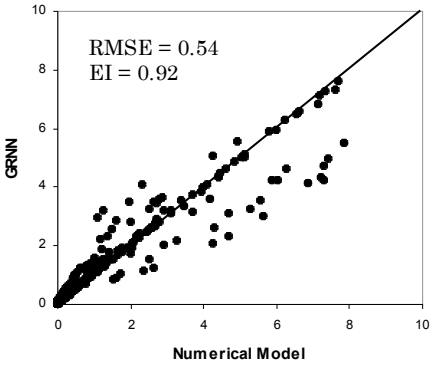


(f) Ko Sarai

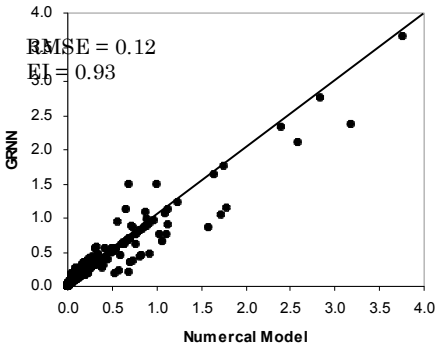


(e) 1st Buoy

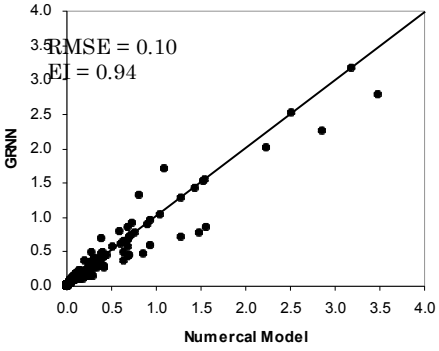


(f) 2nd Buoy

Fig. 6 Scatter plots of Tsunami wave height from GRNN – 1 Model

The outputs of GRNN-1 model in term of arrival time and wave height are stored and displayed on a website. By moving a cursor to the location where the earthquake occurred (Fig. 7a), 2 inputs (Earthquake magnitude and depth) are needed to fill (Fig. 7b). The program then selects a database corresponding to the event and displays the arrival time and wave height in 6 provinces along Thailand's Andaman coastline (Fig. 7c). Then, by moving the cursor to a location of where you are and press enter, the arrival time and wave height for communities at risk in that province will be displayed (Fig. 10d). Therefore, the people in several communities can understand their tsunami vulnerabilities within 5 minutes after the earthquake occurrence and can prepare themselves for safe evacuation according to the tsunami evacuation route map.

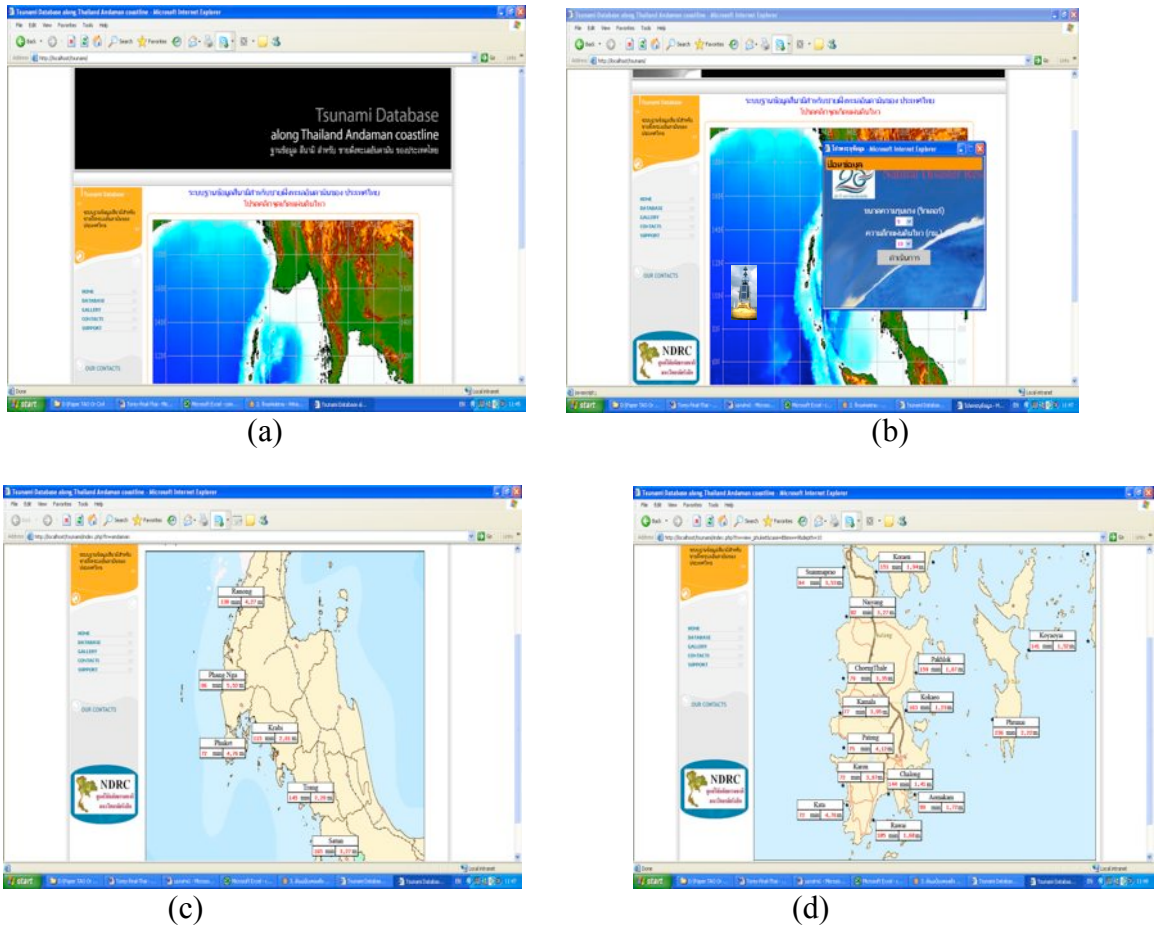


(a) (b)

(c) (d)

Fig. 7 Web-based online tsunami warning system for Thailand's Andaman Coastline

However, in real practice, the confirmation of tsunami wave arrival is one of interesting topics for researchers. Therefore, several false alarms may be expected. In this paper, we try to use the real-time deep sea buoy for making an assessment of the severity of the waves at the risked communities. Therefore, we improved the previous GRNN model (GRNN-1) by including wave height at the DART buoys (Nos. 23401 and 54301) that were installed in the Indian Ocean. The

forecasted outputs of tsunami height at the same 58 communities can be computed as given in Table 5. Scatter plots of tsunami waves at 6 communities same as Fig. 6 is also shown in Figs. 8 to 10.

Table 5 Statistical parameters comparison

| Communities | GRNN-1 Model | | GRNN-1.1 Model | | GRNN-1.2 Model | | GRNN-2 Model | |
|---|---|---|---|---|---|---|---|---|
| | EI | RMSE (m) | EI | RMSE (m) | EI | RMSE (m) | EI | RMSE (m) |
| Klongkong | 0.92 | 0.40 | 0.97 | 0.27 | 0.97 | 0.27 | 0.98 | 0.24 |
| Kaopayam | 0.95 | 0.41 | 0.98 | 0.26 | 0.97 | 0.30 | 0.98 | 0.29 |
| Bangben | 0.92 | 0.39 | 0.97 | 0.27 | 0.97 | 0.27 | 0.97 | 0.24 |
| BanChakle | 0.94 | 0.09 | 0.97 | 0.06 | 0.97 | 0.06 | 0.98 | 0.06 |
| Talaenok | 0.93 | 0.51 | 0.98 | 0.32 | 0.97 | 0.34 | 0.98 | 0.30 |
| Suksamlan | 0.95 | 0.44 | 0.98 | 0.28 | 0.98 | 0.31 | 0.98 | 0.29 |
| BanTream | 0.96 | 0.41 | 0.98 | 0.27 | 0.98 | 0.28 | 0.98 | 0.27 |
| Tunglaaon | 0.95 | 0.17 | 0.98 | 0.11 | 0.98 | 0.11 | 0.98 | 0.12 |
| Tungdab | 0.96 | 0.54 | 0.98 | 0.42 | 0.98 | 0.44 | 0.98 | 0.47 |
| Tungtuk | 0.95 | 0.58 | 0.98 | 0.36 | 0.98 | 0.38 | 0.98 | 0.43 |
| Namkem | 0.94 | 0.60 | 0.98 | 0.40 | 0.98 | 0.41 | 0.98 | 0.38 |
| Bandsak | 0.96 | 0.63 | 0.98 | 0.43 | 0.98 | 0.44 | 0.98 | 0.41 |
| Pakarang | 0.97 | 0.66 | 0.98 | 0.47 | 0.98 | 0.48 | 0.98 | 0.47 |
| Bangniang | 0.97 | 0.73 | 0.98 | 0.57 | 0.98 | 0.60 | 0.98 | 0.59 |
| Tablamu | 0.97 | 0.52 | 0.98 | 0.44 | 0.98 | 0.48 | 0.98 | 0.48 |
| Tabyang | 0.98 | 0.56 | 0.98 | 0.49 | 0.98 | 0.53 | 0.98 | 0.56 |
| Nairai | 0.97 | 0.59 | 0.98 | 0.46 | 0.98 | 0.49 | 0.98 | 0.50 |
| Natai | 0.97 | 0.58 | 0.98 | 0.44 | 0.98 | 0.46 | 0.98 | 0.46 |
| Klong Klain | 0.92 | 0.14 | 0.97 | 0.09 | 0.97 | 0.09 | 0.98 | 0.08 |
| Klongbon | 0.93 | 0.22 | 0.97 | 0.16 | 0.97 | 0.16 | 0.97 | 0.15 |
| Plunai | 0.95 | 0.25 | 0.97 | 0.18 | 0.97 | 0.18 | 0.97 | 0.18 |
| Bangpat | 0.89 | 0.14 | 0.95 | 0.10 | 0.94 | 0.10 | 0.96 | 0.09 |
| SaunMaprawe | 0.97 | 0.56 | 0.98 | 0.42 | 0.98 | 0.42 | 0.98 | 0.45 |
| Naiyang | 0.97 | 0.66 | 0.97 | 0.62 | 0.97 | 0.63 | 0.97 | 0.59 |
| Pasak | 0.97 | 0.50 | 0.98 | 0.39 | 0.98 | 0.39 | 0.98 | 0.41 |
| Kamala | 0.97 | 0.56 | 0.98 | 0.43 | 0.98 | 0.45 | 0.98 | 0.46 |
| Patong | 0.96 | 0.59 | 0.97 | 0.51 | 0.97 | 0.52 | 0.96 | 0.56 |
| Karon | 0.97 | 0.70 | 0.97 | 0.66 | 0.97 | 0.67 | 0.98 | 0.58 |
| Kata | 0.97 | 0.71 | 0.97 | 0.65 | 0.97 | 0.66 | 0.98 | 0.64 |
| Saiyuan | 0.96 | 0.29 | 0.97 | 0.22 | 0.97 | 0.22 | 0.97 | 0.23 |
| Palai | 0.95 | 0.23 | 0.98 | 0.14 | 0.98 | 0.14 | 0.99 | 0.12 |
| Aomakam | 0.94 | 0.23 | 0.98 | 0.14 | 0.98 | 0.14 | 0.98 | 0.12 |
| Bangku | 0.91 | 0.21 | 0.96 | 0.13 | 0.96 | 0.14 | 0.97 | 0.12 |
| Phaklok | 0.93 | 0.24 | 0.98 | 0.14 | 0.98 | 0.14 | 0.98 | 0.12 |
| Kaoaen | 0.93 | 0.58 | 0.95 | 0.45 | 0.95 | 0.47 | 0.96 | 0.44 |
| Leam Sak | 0.87 | 0.19 | 0.94 | 0.14 | 0.93 | 0.14 | 0.95 | 0.12 |
| Tatonglang | 0.91 | 0.30 | 0.96 | 0.19 | 0.96 | 0.19 | 0.97 | 0.17 |
| Khao Kuao | 0.94 | 0.27 | 0.96 | 0.21 | 0.97 | 0.20 | 0.97 | 0.20 |
| Ao Nang | 0.92 | 0.37 | 0.97 | 0.24 | 0.97 | 0.23 | 0.97 | 0.22 |
| Phiphi | 0.94 | 0.43 | 0.96 | 0.35 | 0.96 | 0.35 | 0.96 | 0.36 |

| | | | | | | | | |
|---|---|---|---|---|---|---|---|---|
| Khlong Prasong | 0.89 | 0.20 | 0.96 | 0.13 | 0.95 | 0.14 | 0.97 | 0.12 |
| Khlongruao | 0.87 | 0.27 | 0.95 | 0.18 | 0.95 | 0.18 | 0.96 | 0.16 |
| Khaopu | 0.94 | 0.38 | 0.97 | 0.27 | 0.98 | 0.25 | 0.98 | 0.25 |
| Klongtop | 0.94 | 0.45 | 0.97 | 0.30 | 0.97 | 0.29 | 0.98 | 0.27 |
| Pak Klong | 0.93 | 0.35 | 0.98 | 0.19 | 0.97 | 0.22 | 0.99 | 0.17 |
| Musa | 0.88 | 0.25 | 0.94 | 0.18 | 0.94 | 0.18 | 0.95 | 0.16 |
| Dunun | 0.90 | 0.24 | 0.96 | 0.16 | 0.96 | 0.16 | 0.97 | 0.14 |
| Hang Lang | 0.91 | 0.32 | 0.97 | 0.20 | 0.97 | 0.20 | 0.98 | 0.17 |
| Khao Phul | 0.92 | 0.29 | 0.97 | 0.18 | 0.97 | 0.18 | 0.98 | 0.16 |
| Phla Muang | 0.90 | 0.15 | 0.95 | 0.10 | 0.95 | 0.10 | 0.96 | 0.09 |
| Lang Khao | 0.93 | 0.36 | 0.97 | 0.24 | 0.98 | 0.22 | 0.98 | 0.21 |
| Na Hedchum | 0.91 | 0.20 | 0.96 | 0.14 | 0.96 | 0.14 | 0.97 | 0.12 |
| Na Hedchum | 0.92 | 0.22 | 0.97 | 0.14 | 0.97 | 0.14 | 0.98 | 0.12 |
| Tong Kanan | 0.88 | 0.23 | 0.95 | 0.16 | 0.94 | 0.17 | 0.95 | 0.15 |
| Son Klang | 0.92 | 0.36 | 0.97 | 0.23 | 0.97 | 0.22 | 0.98 | 0.19 |
| Taolosai | 0.91 | 0.20 | 0.96 | 0.14 | 0.96 | 0.14 | 0.97 | 0.12 |
| Klongkike | 0.87 | 0.21 | 0.94 | 0.15 | 0.93 | 0.15 | 0.95 | 0.13 |
| Ko Sarai | 0.93 | 0.49 | 0.97 | 0.31 | 0.97 | 0.31 | 0.98 | 0.26 |
| **Average** | **0.93** | **0.38** | **0.97** | **0.28** | **0.97** | **0.29** | **0.97** | **0.28** |

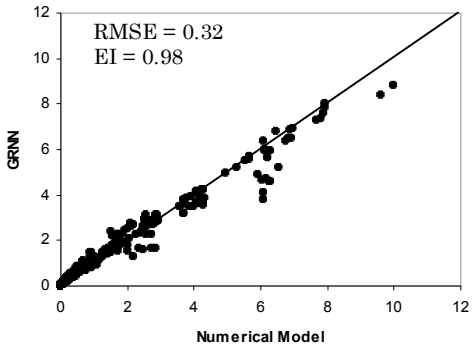


(a) Talaenok

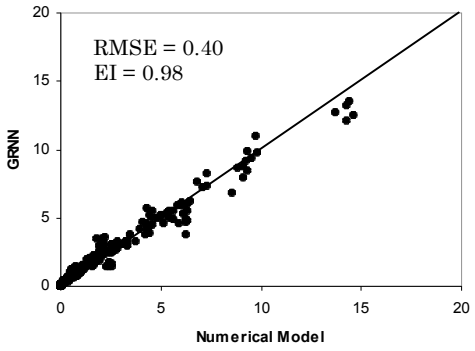


(b) Namkem

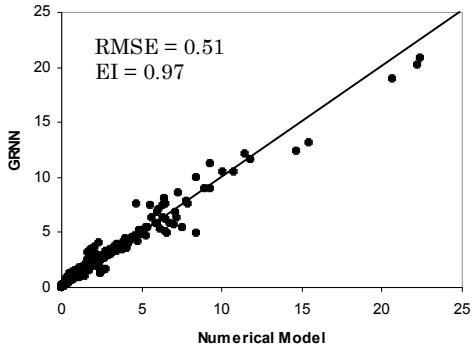


(c) Patong beach

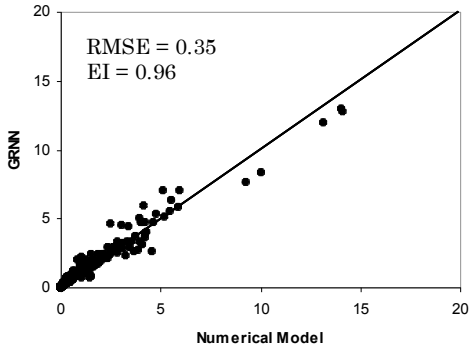


(d) Phiphi Island

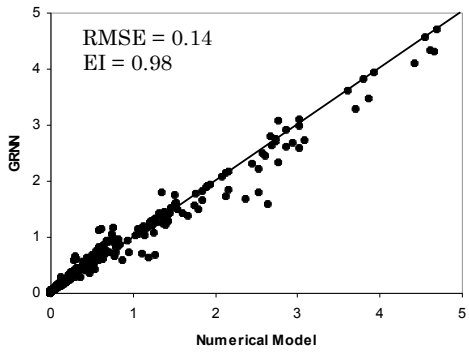


(e) Ao Makam

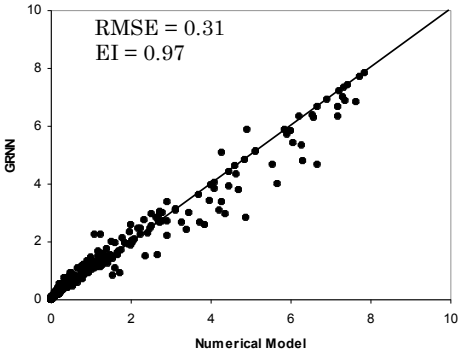


(f) Ko Sarai

Fig. 8 Scatter plots of Tsunami wave height from GRNN – 1.1 Model

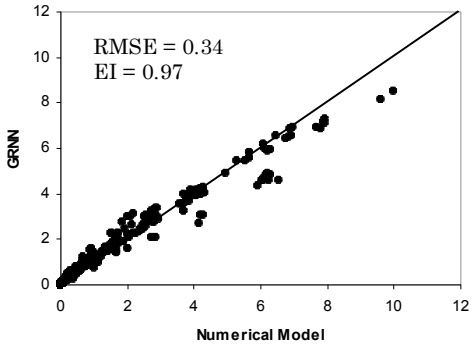


(a) Talaenok

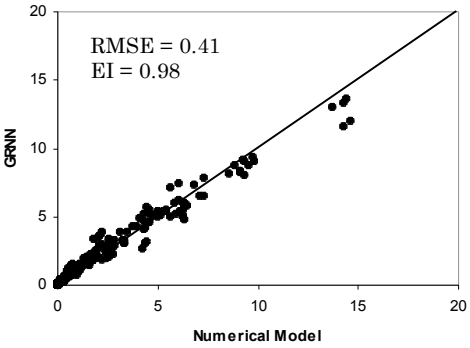


(b) Namkem

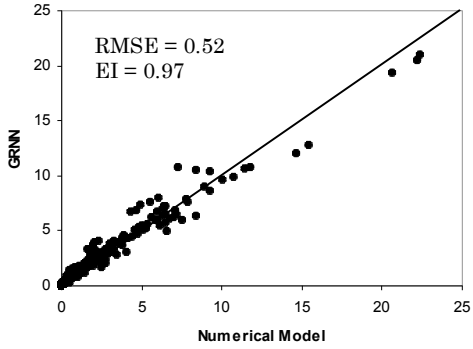


(c) Patong beach

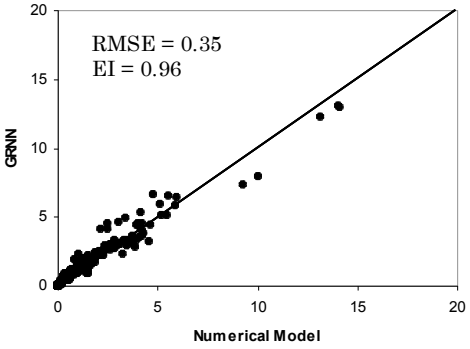


(d) Phiphi Island

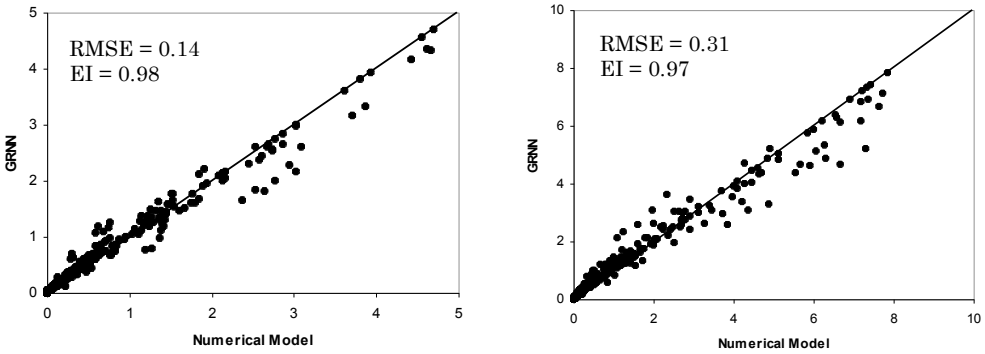


(e) Ao Makam (f) Ko Sarai

Fig. 9 Scatter plots of Tsunami wave height from GRNN – 1.2 Model

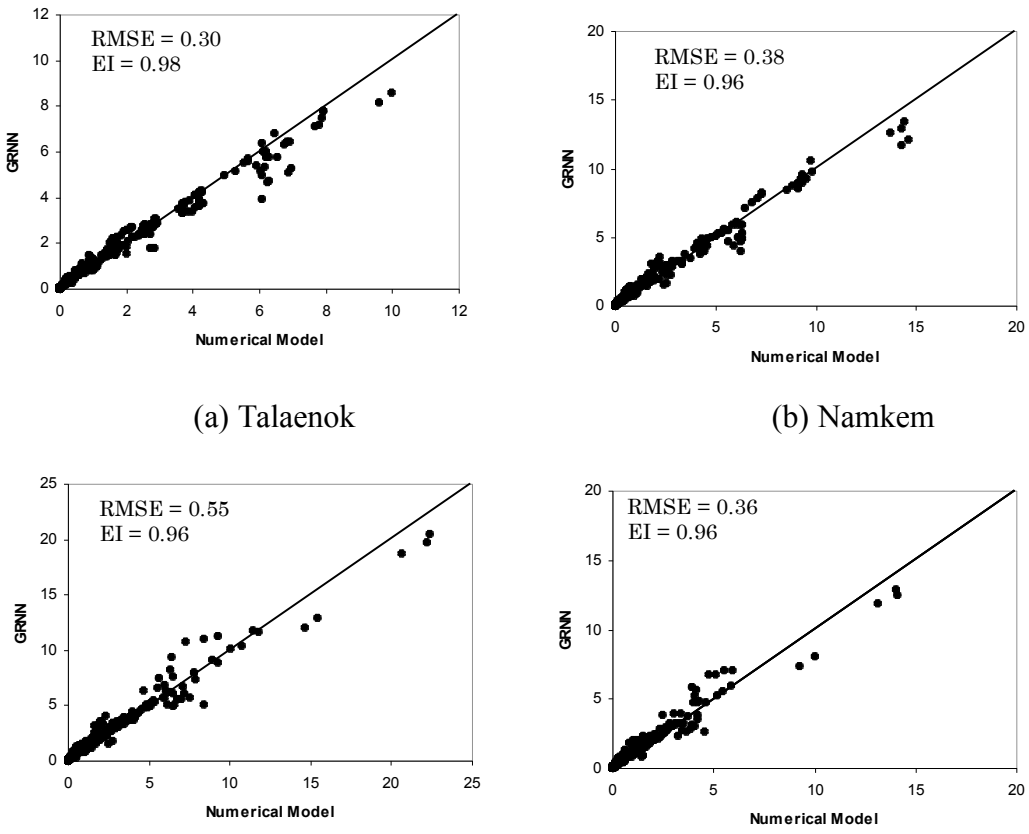


(a) Talaenok (b) Namkem

(c) Patong beach (d) Phiphi Island

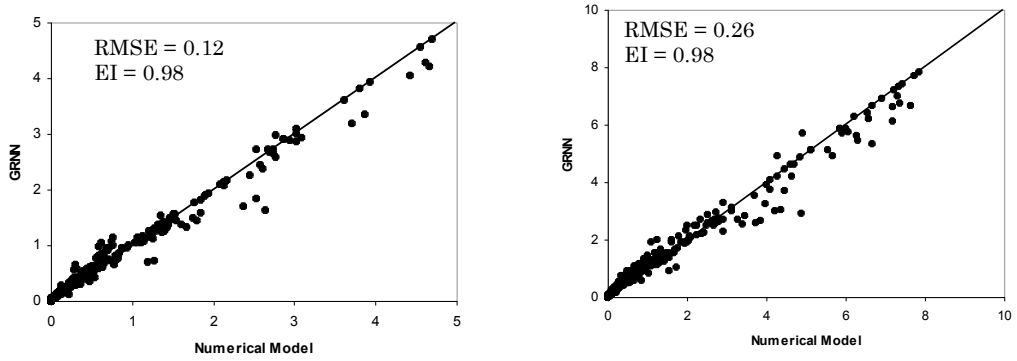


(e) Ao Makam (f) Ko Sarai

Fig. 10 Scatter plots of Tsunami wave height from GRNN -2 Model

It can be seen from Table 6 that, on the average, the EI increases 4 % while the RMSE decreases 26 % for all last 3 models (GRNN-1.1, GRNN-1.2, GRNN-2) compared to the first GRNN model (GRNN-1). These significant improvements of EI and RMSE indicate the essential requirement of real-time monitoring from these buoy data for the confirmation of tsunami warning massages to the people. We could not see significant difference among the last 3 models in Figs. 8 to 10. Therefore, the GRNN-1.1, GRNN-1.2, and GRNN-2 models can be used to compute the updated value of wave heights along 58 communities at risk, depending on the time arrival of wave at the buoys.

## 6. Conclusions

In this study, we present the development of the Tsunami Warning System for Thailand's Andaman Sea coastline by using 3 combination techniques; numerical simulation, GRNN and web base developing, and data assimilation from DART buoys. The numerical simulation (by the linear and non-linear shallow water equations) was carried out from the 420 hypothetical cases of postulated tsunamigenic earthquakes with epicenters on the Andaman micro plate in the Indian Ocean. The outputs are tsunami arrival time and the maximum tsunami wave height at 58 selected communities (along Thailand Andaman coastline) and at 2 locations of DART buoy in the Indian Ocean. The model was calibrated with the data of the tsunamis of 1881, 1941 and 2004. The computed results from the numerical model were used to train and test the GRNN model with only 4 input parameters (latitude, longitude and earthquake magnitude and depth) by the cross training technique. Good accuracy of the forecasted results by the GRNN (GRNN-1) model was found from the efficiency index (EI > 0.90) and the root mean square error (RMSE < .38 m). Then, the results were used to construct the tsunami database which could be displayed on the internet website. Finally, we assimilated the data from two DART buoys in the Indian Ocean to the previous model, thus deriving three additional GRNN (GRNN-1.1, GRNN-1.2, and GRNN-2) models. The additional GRNN models gave a higher performance (EI increases of 4 % and RMSE decreases of 26 %) compared to the GRNN-1 model. The selection of the models is dependent on the arrival time of a tsunami. Thus, thesr models can be used to confirm and update tsunami generation and potential tsunami heights near the epicenter and at Thailand's coastline.

## 7. References


Cigizoglu H. K., Generalized regression neural network in monthly flow forecasting, Civil Engineering and Environmental System, Vol.22, No.2, 71-84. 2005.

Donald L. and Kevin J., New Empirical Relationships among Magnitude Length, rupture width, rupture area and surface Displacement, Bulletin of the Seismological Society of America, Vol. 84, No.4, 997-1002. 1994.

Flood, I., and Kartam, N., Neural networks in civil engineering –I Principles and understanding, Journal of Computing in Civil Engrg., ASCE, Vol. 8, No.2, 131-148. 1994.

Kanamori, H.,1977, The energy release in great earthquakes, Journal of Geophys. Res., 82., pp 1981 – 1987

Hsieh, B. B. and Pratt, T. C., Counter-propagation network, Journal of Applied Optics, Vol. 23, No.6, 4979 – 4984. 2001.

International Federation of Red Cross and Real Crescent Societies, Worlds Disaster Report, Kumarian Press, Bloomfield, Connecticut, pp 246. 2005.

Japan Meteorological Agency, Japan Meteorological Agency - The national meteorological service of Japan, Japan. 2006.

Kowalik, Z. and Murty, T.S, Numerical simulation of two-dimensional tsunami runup. Marine Geodesy, Vol. 16, No.2, 87–100. 1993.

Lay, T., Kanamori, H., Ammon, C., Nettles, M., Ward, S., Aster, R., Beck, S., Bilek, S., Brudzinski, M., Butler, R., DeShon, H., Ekstrom, G., Satake, K. and Sipkin, S., The Great Sumatra-Andaman Earthquake of 26 December 2004, Science, Vol 308, No. 5725, 1127 – 1133. 2005.

Lee, H.-J., Cho, Y.-S.,and Woo, S.-B., Quick tsunami forecasting based on database. IN Satake, Kenji, editor, Tsunamis - Case studies and recent developments, Springer (Dordrecht, The Netherlands), 231-240. 2005.

Mansinha, L and Smylie, D.E, The displacement fields of inclined faults , Ball. Seism. Soc. Auer.61, 1433-1440. 1971.

National Disaster Warning Center, A document for the Tsunami alert rapid notification system (trans) system design and plan workshop, 24th -27th May, Sailom Hotel, Huahin Thailand. 2006.

NOAA's National Geophysical Data Center, http://www.ngdc.noaa.gov/seg/hazard/tsrnsrch_idb.shtml. 2005.

Shuto, N., T. Suzuki, K. Hasegawa, and K. Inagaki, A study of numerical techniques on the tsunami propagation and run-up, Science of Tsunami Hazard, Vol. 4, No.2, 111-124. 1986.

Shuto, N. and Imamura, F., IUGG/IOC time project, numerical method of tsunami simulation with the leap-frog scheme manuals and guides, UNESCO' s Workshop, Paris. 1997.

Specht, D.F., A General Regression Neural Network, IEEE trans on Neural Networks, Vol. 2, No. 6, 568 – 576. 1991.

Supharatid, S., Tidal-level forecasting and filtering by neural network model, Coastal Engineering Journal, Vol 45, No. 1, 119-138. 2003.

Titov, V.V. and C.E. Synolakis. Numerical modeling of tidal wave runup. Journal of Waterways, Ports, Coastal and Ocean Engineering Vol. 124, No.4, 157-171. 1998.

Titov, V.V., F.I. González, E.N. Bernard, M.C. Eble, H.O. Mofjeld, J.C. Newman, and A.J. Venturato. Real-time tsunami forecasting: Challenges and solutions, Natural Hazards Vol. 35, No. 1, 41-58. 2005.

Whitmore, P. M. and Sokolowski, T. J. Predicting tsunami amplitudes along the North American coast from tsunamis generated in the northwest Pacific Ocean during tsunami warnings, Science of Tsunami Hazards, Vol. 14, No. 3, 147-166. 1996.